

Lowest Fatigue Limit Estimation of Ductile Cast Iron Joints by Considering Maximum Defect Size Toward Replacing Welded Joints

Tetsuro HIDAKA,^{1)*} Nao-Aki NODA,²⁾ Yoshikazu SANO,²⁾ Nobuhiro KAI¹⁾ and Hiroyoshi FUJIMOTO¹⁾

1) Research and Development Center, HINODE, Ltd., Iwasaki, Harakoga, Miyaki-cho, Miyaki-gun, Saga, 849-0101 Japan.

2) Dept. of Mechanical and Control Engineering, Kyusyu Institute of Technology, 1-1 Sensui-cho, Tobata-ku, Kitakyusyu, Fukuoka, 804-8550 Japan.

(Received on August 20, 2019; accepted on November 18, 2019; originally published in *Tetsu-to-Hagané*, Vol. 105, 2019, No. 9, pp. 877–886; J-STAGE Advance published date: January 18, 2020)

In our earlier study, the authors revealed that the fatigue limit of ductile cast iron (DCI) specimens whose shapes are similar to the welded joint shapes is about three times larger than that of the welded joint specimens. However, since many defects are usually included in the DCI specimens, the fatigue limit of DCI joints decreases with increasing the maximum defect size. In this paper, therefore, the maximum defect size is estimated by using statistics of extremes. Then, the lowest fatigue limit corresponding to the maximum defect size is estimated from the 4 parameter model and compared with the lowest fatigue limit of the welded joint. As a result, it was confirmed that the lowest fatigue limit of the DCI specimens is about twice as large as the welded joint.

KEY WORDS: fatigue strength; ductile cast iron; welded joint; statistics of extremes; 4 parameter model; $\sqrt{\text{area}}$ parameter model.

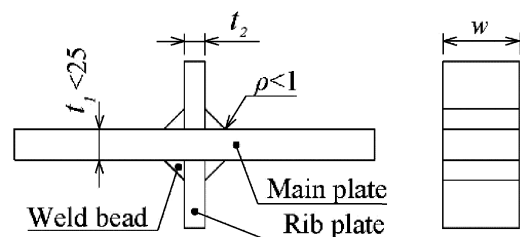
1. Introduction

Ductile cast iron (DCI)^{1,2)} has attracted attention as a material that can replace welded joints.³⁾ In our previous experimental study, the authors revealed that the fatigue strength of DCI joints is about 2 times or more larger than that of non-load-carrying cruciform welded joints.⁴⁾ Hereafter, non-load-carrying cruciform welded joint is referred to welded joint or cross welded joint. Then, the large fatigue strength of DCI joints is theoretically explained in terms of stress concentration factor, notch insensitivity and residual stress.⁴⁾ However, in our previous study,⁴⁾ the defect size was not considered although many defects included in DCI joints cause fatigue crack initiation.

Therefore, in this study, the effect of the defects on the fatigue strength for DCI joints will be investigated. It is known that the maximum defect size increases with increasing specimen thickness. Therefore, the fatigue test will be carried out by varying the thickness of DCI joints. Then, the defect size causing the final fracture will be investigated under various stress amplitude. Based on the defect size distribution, the maximum defects size will be estimated theoretically for DCI joints by using statics of extremes. Then, the lowest fatigue strength of DCI joints obtained from the maximum defect size will be compared with the lowest fatigue strength of the welded joints.

2. Fatigue Strength Characteristics of Non-load-carrying Cruciform Welded Joints

Figure 1 shows shape of the welded joint. **Figure 2** shows the macrostructure of the welded portion. It is known that the fatigue strength of the welded joint decreases with increasing the main plate thickness t_1 and rib thickness t_2 . For example, the fatigue strength decreases 40 MPa with increasing $t_1 = 10$ mm to 20 mm.⁵⁾ It is also known that the effect of plate width w on the fatigue strength is small.⁵⁾ This is because fatigue strength is most affected by the stress concentration factor K_t at the weld toe, which is determined by the main plate thickness t_1 , rib thickness t_2 and the weld toe radius ρ .⁶⁾ **Figure 3** shows fatigue design curves of welded joints;^{7,8)} one is prescribed by Japanese Society of Steel Construction (JSSC) and the other is by International Institute of Welding (IIW). The JSSC-E curve in Fig. 3 named E class has lowest fatigue strengths



Material: SM(JIS G 3106) et al.

Fig. 1. Shape of welded joints.

* Corresponding author: E-mail: t-hidaka@hinodesuido.co.jp
DOI: <https://doi.org/10.2355/isijinternational.ISIJINT-2019-494>

$\sigma_f^{JSSC} = 80 \text{ MPa}$ at $N = 2 \times 10^6$ and $\sigma_{low}^{JSSC} = 62 \text{ MPa}$ at $N = 10^7$. The fatigue test shows that more than 97.7% of 467 specimens are stronger than the JSSC-E curve shown in Fig. 3. In this way, the JSSC-E curve is recommended to be used in fatigue design of cross welded joints in Japan. Similarly, the IIW-FAT80 curve in Fig. 3 is named FAT80 has fatigue strengths $\sigma_f^{IIW} = 80 \text{ MPa}$ at $N = 2 \times 10^6$ and $\sigma_{low}^{IIW} \cong 50 \text{ MPa}$ at $N = 10^7$. This curve also can be used in fatigue design of cross welded joints as prescribed by International Institute of Welding (IIW).

From the above discussion, the lowest fatigue strength of JSSC-E ($\sigma_{low}^{JSSC} = 62 \text{ MPa}$) of cross welded joint will be compared with the lowest fatigue strength of DCI joint. This is because fatigue strength of JSSC-E is larger than that of IIW-FAT80. The JSSC-E curve can be applied under the following condition when tensile strength $\sigma_B < 570 \text{ MPa}$, main plate thickness $t_1 < 25 \text{ mm}$, the weld toe radius $\rho \leq 1 \text{ mm}$ and toe treatment is as weld.⁹⁾

In our previous study, the fatigue strength of DCI joint was experimentally obtained and compared with the fatigue strength of the welded joint when the average weld toe radius $\rho = 0.485 \text{ mm}$ is smaller than the general weld toe radius.⁴⁾ Therefore, in this study, more general results will be studied by estimating the lowest strengths. First, the lowest fatigue strength of DCI joints will be estimated. Then, the results will be compared with the lowest fatigue strength estimated by Japanese Society of Steel Construction (JSSC).

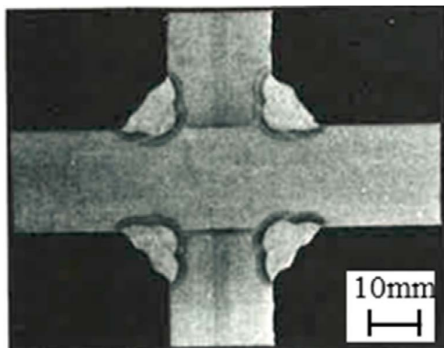


Fig. 2. Macrostructure of welded portion (Etched by nital). (Online version in color.)

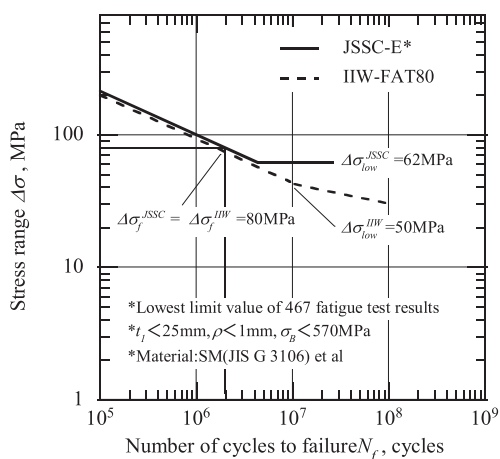


Fig. 3. S-N diagram showing fatigue design curve defined by JSSC and IIW in Fig. 1.

3. Fatigue Test Results of DCI Joints

3.1. DCI Joints Fatigue Test Specimen

Figure 4 shows the specimen dimensions. To investigate the effect of the defect size and the stress concentration, the main plate thickness $t_1 = 6, 12, 24 \text{ mm}$ will be considered. Here, the smallest thickness $t_1 = 6 \text{ mm}$ is empirically chosen as a minimum thickness which can be manufactured for small and medium-sized castings. The largest thickness $t_1 = 24 \text{ mm}$ is chosen as the maximum thickness within the application range of the fatigue design curve JSSC-E in Fig. 3. The main plate thickness $t_1 = 12 \text{ mm}$ is chosen as a middle thickness between the smallest and largest thickness. Since the other dimensions are the same as the ones in the previous study,⁴⁾ the details are not indicated in this paper. Note that the test specimen has a casting surface with shot blasting for sand removal. Here, the fatigue strength with shot blasting is improved by the compressive residual stress.⁴⁾ The rib thickness t_2 also has a large effect on the fatigue strength, but this paper assumes a constant value $t_2 = 16 \text{ mm}$. The effect of t_2 will be considered in further study.

Table 1 shows the chemical composition of DCI joints. Table 2 shows the mechanical properties of DCI joints. The tensile strength of DCI joints $\sigma_B = 560 \text{ MPa}$ is within the applicable range ($\sigma_B < 570 \text{ MPa}$) of the fatigue design curve JSSC-E in Fig. 3 to be compared. Figure 5 shows the microstructures of DCI joints. These test specimens

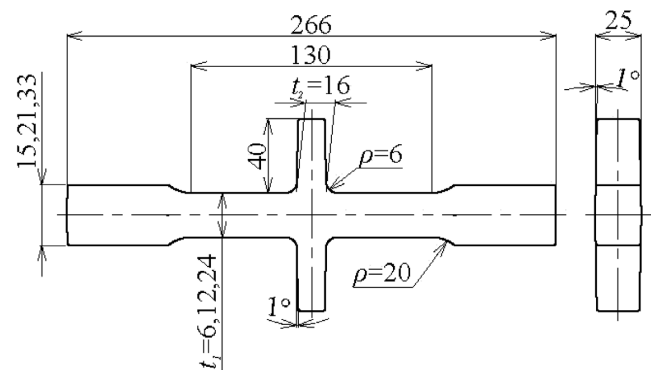


Fig. 4. Dimension of DCI joints.

Table 1. Chemical composition of DCI joints (wt%).

Main plate thickness t_1 (mm)	C	Si	Mn	P	S	Cu	Mg
6	3.63	2.46	0.40	0.020	0.002	0.32	0.039
12	3.73	2.53	0.41	0.022	0.002	0.31	0.047
24	3.67	2.45	0.41	0.024	0.004	0.31	0.042

Table 2. Mechanical properties of DCI joints.

Main plate thickness t_1 (mm)	JIS Z 2241(2017), No. 14B type tensile test specimen			
	0.2% Proof stress (MPa)	Tensile strength (MPa)	Elongation (%)	Brinell hardness (HB)
6	361	557	7.0	192
12	339	561	14.5	190
24	340	560	15.8	191

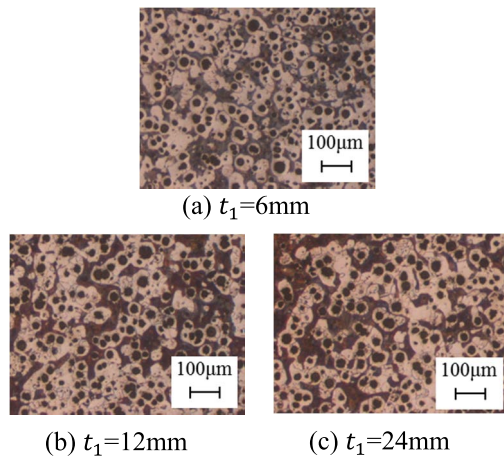


Fig. 5. Microstructure of DCI joints (Etched by nital). (a) $t_1=6$ mm, (b) $t_1=12$ mm, (c) $t_1=24$ mm. (Online version in color.)

have bull's eye structure, which are usually found in general ductile cast iron, independent of the main plate thickness t_1 .

3.2. Fatigue Test Condition

The fatigue load was conducted under the axial tensile loading with $R=0$ in accordance with the test condition for the welded joint. An electro-hydraulic servo fatigue tester (manufactured by MTS) having a load capacity of ± 100 kN was used as a fatigue testing machine. The repetitive waveform was a sine wave, and the frequency was 5 to 30 Hz. Fatigue test was carried out in the atmosphere at room temperature ($23 \pm 3^\circ\text{C}$). The applied maximum stress is changed by decreasing gradually from 350–400 MPa considering the specimen's 0.2% proof stress. Then, the fatigue test was performed up to the number of cycles $N_f=10^7$.

3.3. Fatigue Test Results of DCI Joint

Figure 6 shows the fatigue test results of DCI joints. The solid line shows S-N diagram obtained by connecting the fatigue strength at finite life and the fatigue strength at the number of cycles $N_f=10^7$. Usually the fatigue strength at finite life is obtained as an average strength passing through the center of several plots.¹¹⁾ However, since Fig. 6 should be compared with Fig. 3 prescribed by JSSC-E for the welded joint, the lower limit of DCI joint strength is also considered in Fig. 6. Fatigue strength at the number of cycles $N_f=10^7$ is obtained as the higher limit of DCI joint strength in Fig. 6. The experimental results in Fig. 6 are numbered from the largest stress amplitude $\Delta\sigma$ to the smallest one. The asterisk '*' in Fig. 6 means another stress amplitude 300 MPa was newly applied to the specimen which is not fractured under the original stress amplitude.

As shown in Fig. 6, the fatigue strength of DCI joints is obtained as $\Delta\sigma_{t=6}^{DCI}=220$ MPa, $\Delta\sigma_{t=12}^{DCI}=240$ MPa and $\Delta\sigma_{t=24}^{DCI}=220$ MPa. These differences are within 20 MPa, and therefore, the fatigue strength of DCI joints does not decrease very much with increasing the main plate thickness t_1 . On the other hand, the fatigue strength of welded joint decreases 40 MPa with increasing $t_1=10$ mm to 20 mm. It is seen that the effect of t_1 on the fatigue strength of DCI joints is smaller than that of welded joints. Note that the fracture position varies depending on plate thickness t_1 . This will be

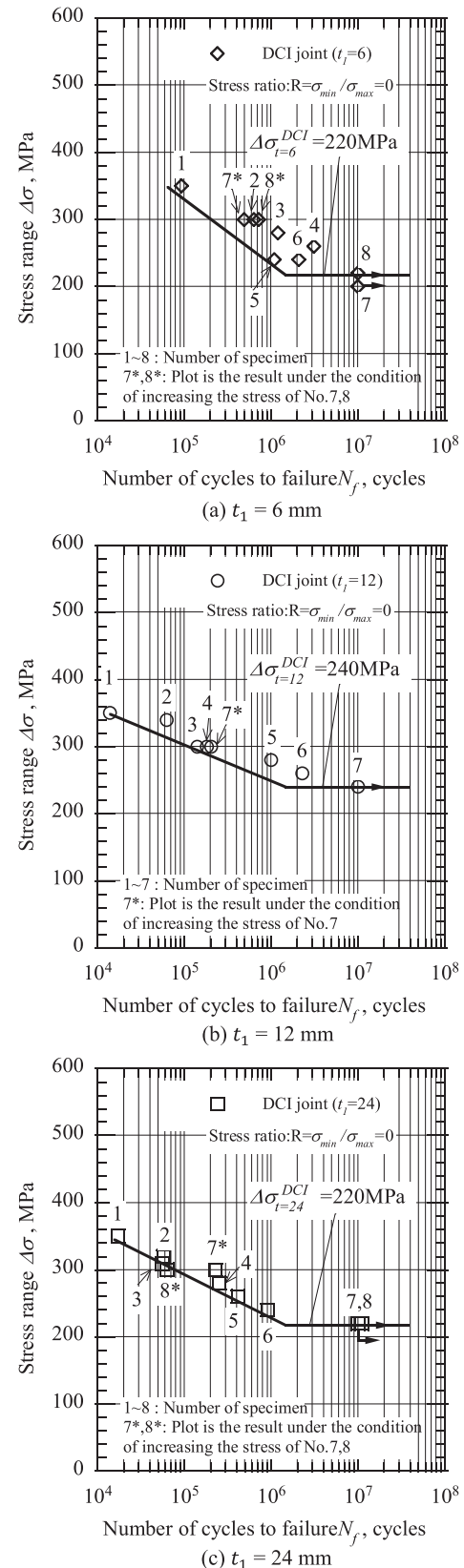


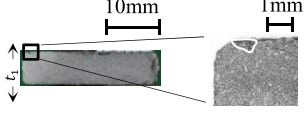
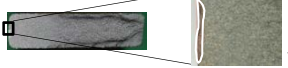
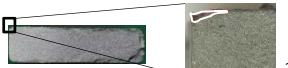





Fig. 6. S-N diagram showing fatigue properties of DCI joints in Fig. 4. (a) $t_1=6$ mm, (b) $t_1=12$ mm, (c) $t_1=24$ mm.

discussed in detail in the next section.

4. Defect Size and Fracture Position of DCI Joint

Tables 3–5 show fracture position, fracture origin and defect size of DCI joints identified from the fracture surface.

Table 3. Fatigue test data of DCI joints ($t_1 = 6$ mm) in Fig. 6(a). (Online version in color.)

No.	$\Delta\sigma$ (MPa)	N_f (cycles)	Broken position in Fig. 7	Fracture origin and defect size: \sqrt{area} (μm)
1	350	9.36×10^4	B	 Inclusions $\sqrt{area}=469$
2	300	6.31×10^5	B	 Surface notch $\sqrt{area}=583$
3	280	1.21×10^6	B	 Surface notch $\sqrt{area}=480$
4	260	3.11×10^6	B	 Inclusions $\sqrt{area}=1104$
5	240	1.09×10^7	B	 Surface notch $\sqrt{area}=943$
6	240	2.09×10^6	B	 Surface notch $\sqrt{area}=656$
7	200	1.00×10^7	—	 Surface notch $\sqrt{area}=1157$
7*	300	4.92×10^5	B	
8	220	1.00×10^7	—	 Surface notch $\sqrt{area}=728$
8*	300	7.20×10^5	B	

As shown in Fig. 7, the fracture position is classified into three groups, that is, fillet portion 'A' near the rib cross-section where stress concentration occurs, smooth portion 'B' and gripped portion 'C' with fillet. To discuss the defect size effect later, Tables 3–5 show values of \sqrt{area} .¹²⁾ Here, \sqrt{area} is the square root of the projected area of the defect onto a plane perpendicular to the maximum principal stress. The specimen number in Tables 3–5 is corresponding to the number in Fig. 6. The symbol '—' means the data will be used for statistic of extremes described later.

Table 3 shows when the main plate thickness $t_1 = 6$ mm, the fracture positions of all specimens are smooth portion B in Fig. 7. Table 4 shows when $t_1 = 12$ mm, most of the fracture positions are smooth portion B except No. 2 specimen fractured at fillet portion A. Table 5 shows when $t_1 = 24$ mm, the fracture positions are fillet portion A or gripped portion C in Fig. 7. When $t_1 = 6$ mm, the fracture origin is the surface notch of the casting surface. When $t_1 = 12, 24$ mm, the fracture origin is the inclusion near the casting surface.

Tables 3–5 show the fracture position varies depending on the main plate thickness. The reason can be explained from the stress intensity factor K_I , which is determined by the stress concentration factors and the defect size at the fractured portion. Since the stress states can be clearly identified at positions A and B, the results at position C are excluded. It is known that the stress concentration factor

at fillet portion A increases with increasing the main plate thickness t_1 . The defect size is also affected by the main plate thickness t_1 .

The stress intensity factor K_I can be expressed as shown in Eq. (1).^{13,14)} Here, σ_0 is the nominal stress, \sqrt{area} is the projected defect size, 0.65 is a correction factor determined by the position where the defect occurs. Assuming that σ_{w0} is the stress at B in Fig. 7, the stress intensity factor of the smooth portion K_I^B can be expressed by Eq. (2). On the hand, the stress intensity factor at A in Fig. 7 is expressed as shown in Eq. (3).

$$K_I = \sigma_0 \sqrt{\pi \sqrt{area}} \quad \text{..... (1)}$$

$$K_I^B = \sigma_{w0} \sqrt{\pi \sqrt{area}^B_{AVE}} \quad \text{..... (2)}$$

$$K_I^A = K_I^A \sigma_{w0} \sqrt{\pi \sqrt{area}^A_{AVE}} \quad \text{..... (3)}$$

K_I : Stress intensity ($\text{MPa}\sqrt{\text{m}}$)

K_I^B : Stress intensity at B ($\text{MPa}\sqrt{\text{m}}$)

K_I^A : Stress intensity at A ($\text{MPa}\sqrt{\text{m}}$)

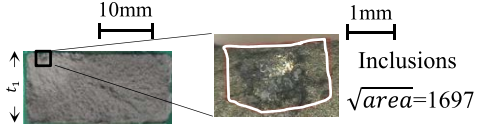


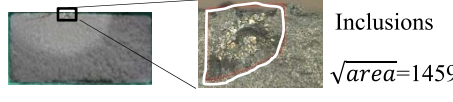



σ_0 : Nominal stress (MPa)

σ_{w0} : Stress at B (MPa)

\sqrt{area} : Defect size (μm)

\sqrt{area}^B_{AVE} : Mean defect size at B (μm)

Table 4. Fatigue test data of DCI joints ($t_1 = 12$ mm) in Fig. 6(b). (Online version in color.)

No.	$\Delta\sigma$ (MPa)	N_f (cycles)	Broken position in Fig. 7	Fracture origin and defect size: \sqrt{area} (μm)
<u>1</u>	350	1.39×10^4	B	
2	340	6.29×10^4	A	
<u>3</u>	300	1.41×10^5	B	
<u>4</u>	300	1.81×10^6	B	
<u>5</u>	280	1.00×10^6	B	
<u>6</u>	260	2.27×10^6	B	
<u>7</u>	240	1.00×10^7	—	
7*	300	2.03×10^5	B	

\sqrt{area}_{AVE}^A : Mean defect size at A (μm)
 K_t^A : Stress concentration factor at A

Here, the stress at B was the fatigue limit for each main plate thickness t_1 , $\sigma_{w0} = 220$ MPa when $t_1 = 6, 24$ mm, and $\sigma_{w0} = 240$ MPa when $t_1 = 12$ mm. $\sqrt{area}_{AVE}^{A,B}$ is the average value of the defect size at each of the fracture positions A or B. Since the fracture position of $t_1 = 6$ mm was all B, the defect size at A is unknown. Therefore, the defect size at A \sqrt{area}_{AVE}^A is used value of $t_1 = 12$ mm (Table 4, No. 2). Then, since the specimen of $t_1 = 24$ mm is not fractured at B, \sqrt{area}_{AVE}^B is used the maximum defect size of $t_1 = 24$ mm (Table 5, No. 2). The stress concentration factor K_t^A is defined as $K_t = \sigma_{max} / \sigma_n$. Here, σ_{max} is the maximum stress at A and σ_n is the nominal stress at B.

Table 6 shows calculation result of K_t at each fracture position A and B. In Table 6, K_t^A / K_t^B is indication to be estimated the fracture position. In other words, $K_t^A / K_t^B < 1$, it means that the specimen is likely to fracture at the smooth portion B. While, $K_t^A / K_t^B > 1$, it means that the specimen is likely to fracture at the fillet portion of the rib cross-section A. From the above, all specimens of $t_1 = 6$ mm is fractured at B. This is because $K_t^A / K_t^B = 0.64 < 1$. The most specimens of $t_1 = 12$ mm are fractured at B. This is because $K_t^A / K_t^B = 0.63 < 1$. The specimens of $t_1 = 24$ mm tend to be fractured at A. This is because $K_t^A / K_t^B = 1.30 > 1$.

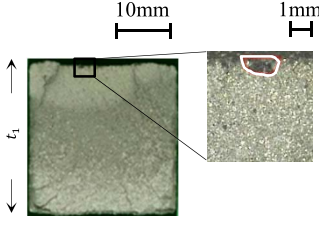
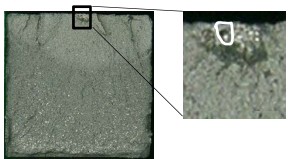
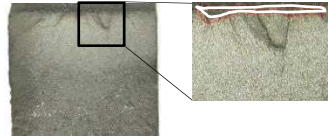
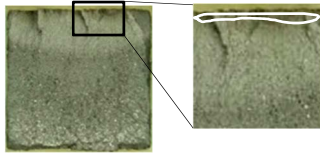

5. Fatigue Strength Comparison of DCI Joint and the Cross Welded Joint

The fatigue strength of DCI joints shown in chapter 4 is limited to the case where the defect size is in the range shown in Tables 3 to 5. Therefore, if the number of specimens is increased, defect size is larger and the fatigue strength is decreased. From the above, in this chapter, the maximum defect size of DCI joint will be estimated by statistics of extremes. Then, the lowest fatigue strength of DCI joint will be compared with that of the cross welded joint.

5.1. Maximum Defect Size of DCI Joint

Generally speaking, to estimate the maximum defect size by applying statistics of extremes, the dimensions of the same type of defects appearing at the same portion are collected without using different types of defects.¹⁵⁾ As shown in Table 3, all specimens except No. 1 and 4 of $t_1 = 6$ mm were fractured originating from surface notch near casting surface where occurred at the smooth portion B (See Fig. 7). Therefore, the defect sizes of specimen No. 2, 3, 5 to 8 are the target data for statistics of extremes. As shown in Table 4, $t_1 = 12$ mm, the defect sizes of specimen No. 1, 3 to 7 are the target data. As shown in Table 5, $t_1 = 24$ mm, the defect sizes of specimen No. 1, 3, 5 to 7 are the target data. This is because these defects are all the same kind of inclusions, and the occurrence portions of defects are also the same.

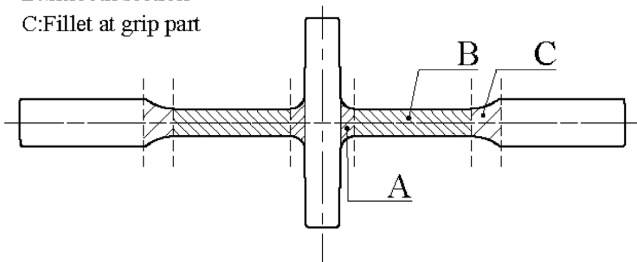
Table 5. Fatigue test data of DCI joints ($t_1=24$ mm) in Fig. 6(c). (Online version in color.)

No.	$\Delta\sigma$ (MPa)	N_f (cycles)	Broken position in Fig. 7	Fracture origin and defect size: \sqrt{area} (μm)	
1	350	1.72×10^4	A		Inclusions $\sqrt{area}=943$
2	320	5.77×10^4	C		Inclusions $\sqrt{area}=1470$
3	310	5.58×10^4	A		Inclusions $\sqrt{area}=886$
4	280	2.52×10^5	C		Inclusions $\sqrt{area}=700$
5	260	4.14×10^5	A		Inclusions $\sqrt{area}=735$
6	240	9.05×10^5	A		Inclusions $\sqrt{area}=916$
7	220	1.00×10^7	—		Inclusions $\sqrt{area}=1005$
7*	300	2.28×10^5	A		
8	220	1.00×10^7	—		Inclusions $\sqrt{area}=1456$
8*	300	6.37×10^4	C		

A: Fillet at rib intersection

B: Smooth section

C: Fillet at grip part


Fig. 7. Classification of broken position of DCI joints.

Note that, the specimens of $t_1=24$ mm which are fractured at fillet portion of the gripping portion C (See Fig. 7), specimen No. 2, 4, 8, is excluded for consideration of statistics of extremes. This is because there is little defect sizes data, the stress condition is different from the intended condition.

The number of specimens for DCI joint for statistics of extremes is set to be larger than that of the cross welded joint. For this reason, the number of specimens for DCI joint is set to 467 for each main plate thickness t_1 . 467 are number of specimens which are determined the lowest fatigue strength of $t_1 < 25$ mm for the cross welded joint (See Fig.

Table 6. Average value of defect size, stress concentration factor and stress intensity factor at each location in Fig. 7.

Main plate thickness t_1 (mm)	A, B: Location in Fig. 7, σ_{w0} : Fatigue limit in Fig. 6, \sqrt{area}_{AVE} : Average value of defect size, K_t : Stress concentration factor, K_I : Stress intensity factor								
	A in Fig. 7				B in Fig. 7				
	σ_{w0} (MPa)	\sqrt{area}_{AVE}^A (μm)	K_t^A	K_I^A (MPa $\sqrt{\text{m}}$)	σ_{w0} (MPa)	\sqrt{area}_{AVE}^B (μm)	K_t^B	K_I^B (MPa $\sqrt{\text{m}}$)	K_I^A / K_I^B
6	220	196*	1.27	4.5	220	765	1.00	7.0	0.64
12	240	196	1.53	5.9	240	1 150	1.00	9.36	0.63
24	220	897	1.68	12.7	220	1 470**	1.00	9.8	1.30

*Assumed value from Table 4 specimen No. 2 **Assumed value from Table 5 specimen No. 2

3). Therefore, this condition is more extensive than that of the cross welded joint. Then, we will consider the control volume per specimen V . The specimens of $t_1=6, 12$ mm which were fractured at the smooth portion B are assumed the control volume V^B to be the depth to 2 mm from the surface (See Fig. 8(a)). This is because fracture origin at the smooth portion B is the inclusion at the depth to 2 mm from the surface. While, it is recommended that the control volume V where the stress concentration exists is that where $\sigma \geq 0.8\sigma_{max}$.^{15,16)} Here, σ is stress generated and σ_{max} is the maximum stress in the control volume. Therefore, the specimens of $t_1=24$ mm which were fractured at the fillet portion of rib cross-section A are assumed the control volume V^A to be 2 mm in depth and 4 mm in width (See Fig. 8(b)). According to the analysis results⁴⁾ performed in our earlier study, the stress condition of V^A is $\sigma \geq 0.7\sigma_{max}$. It is appropriate as the control volume.

From the above, Fig. 9 shows the result for statistics of extremes. In this figure, reduced variate y_i , cumulative frequency F_i , return period T is calculated by the following Eqs. (4) to (6).^{17,18)} As shown in Fig. 9, when $t_1=6$ mm and $T=467$, the defect size $\sqrt{area}_{max}=2\ 605\ \mu\text{m}$. When $t_1=12$ mm, $\sqrt{area}_{max}=3\ 976\ \mu\text{m}$. When $t_1=24$ mm, $\sqrt{area}_{max}=1\ 598\ \mu\text{m}$. These estimated defect sizes are 2 to 8 times larger than experimental defect sizes occurred on fatigue fracture surface.

$$y_i = -\ln[\ln(F_i)] \dots\dots\dots (4)$$

$$F_i = i / (n + 1) \cdot 100 \dots\dots\dots (5)$$

$$T = V_E / V = N V / V = 467 \dots\dots\dots (6)$$

y_i : Reduced variate

F_i : Cumulative frequency (%)

T : Return period

i : Specimen No.

n : Total number of specimens

V_E : Total control volume to estimate

N : Total number of specimens to estimate ($N=467$)

V : Control volume of one specimen

5.2. Lowest Fatigue Limit for DCI Joint

The lowest fatigue limit estimated from \sqrt{area}_{max} estimated in the previous section will be compared with that of the cross welded joint. It is known that \sqrt{area} parameter model¹⁹⁻²¹⁾ and 4 parameter model^{22,23)} is the method for estimating the fatigue limit of defective materials. 4 param-

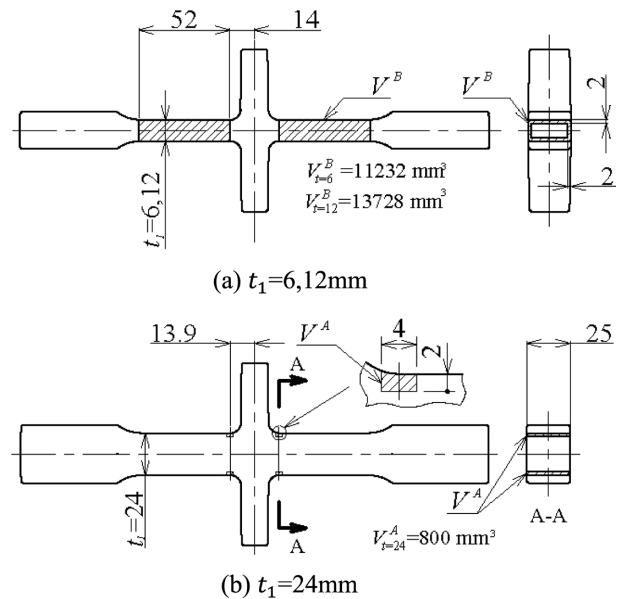


Fig. 8. Control volume V of one DCI joint. (a) $t_1=6, 12$ mm, (b) $t_1=24$ mm.

eter are tensile strength σ_B , Vickers hardness HV , threshold stress intensity factor K_{th} and defect size \sqrt{area} . Here, \sqrt{area} parameter model can be applied to small defects and cracks. However, when $\sqrt{area} > 1\ 000\ \mu\text{m}$, the estimated value may be larger than the actual fatigue limit.²⁴⁾ While, 4 parameter model can be applied in the range of $\sqrt{area} > 1\ 000\ \mu\text{m}$. Since \sqrt{area}_{max} estimated in previous section is larger than $1\ 000\ \mu\text{m}$, in this section, 4 parameter model will be used for the lowest fatigue limit.

As shown by Eqs. (7) to (10),¹⁹⁻²³⁾ the fatigue limit prediction equation of 4 parameter model is defined for each of the three regions determined by the defect size. Here, In the region I, the fatigue limit is proportional to the tensile strength σ_B . In the region II, the fatigue limit is proportional to Vickers hardness HV . The region. As can be seen in Eq. (8), in the region II, the fatigue limit is estimated by \sqrt{area} parameter model. Then, in the region III, since the defect size is larger, the fatigue limit is proportional to threshold stress intensity factor K_{th} .

$$\text{Region I } \sigma_w = 0.48\sigma_B \dots\dots\dots (7)$$

$$\text{Region II } \Delta\sigma = 2 \cdot \sigma_w = \frac{1.41(HV + 120)}{(\sqrt{area})^{1/6}} \cdot \left[\frac{(1-R)}{2} \right]^\alpha \dots\dots\dots (8)$$

$$\alpha = 0.226 + HV \cdot 10^{-4} \dots\dots\dots (9)$$

$$\text{Region III } \Delta\sigma = 2 \cdot \sigma_w = \frac{\Delta K_{th}}{0.65 \sqrt{\pi} \sqrt{area} \cdot 10^{-6}} \dots (10)$$

σ_w : Fatigue limit indicated by stress amplitude (MPa)

$\Delta\sigma$: Fatigue limit indicated by stress range (MPa)

σ_B : Tensile strength (MPa)

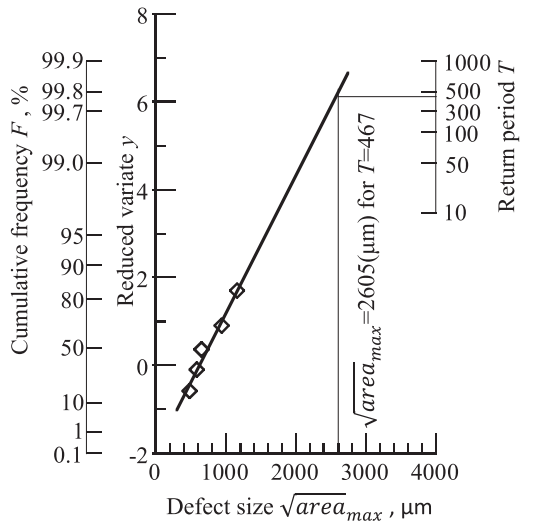
HV : Vickers hardness (HV)

\sqrt{area} : Square root of the projected area of the defect onto a plane perpendicular to the maximum principal stress (μm)

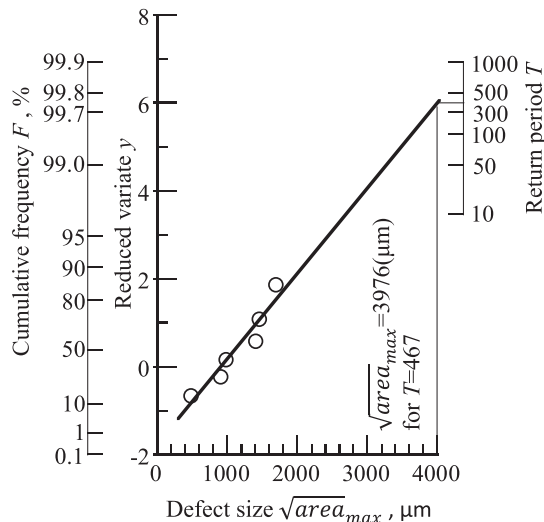
R : Stress ratio

α : Constant defined by HV

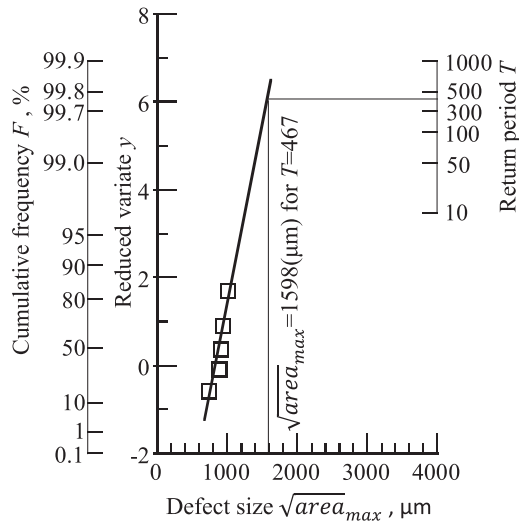
ΔK_{th} : Threshold stress intensity factor ($\text{MPa}\sqrt{\text{m}}$)



(a) $t_1 = 6 \text{ mm}$ ($V = V^B$ in Fig. 8(a))



(b) $t_1 = 12 \text{ mm}$ ($V = V^B$ in Fig. 8(a))



(c) $t_1 = 24 \text{ mm}$ ($V = V^A$ in Fig. 8(b))

Fig. 9. Statistics of extremes of defects occurred in DCI joints. (a) $t_1 = 6 \text{ mm}$ ($V = V^B$ in Fig. 8(a)), (b) $t_1 = 12 \text{ mm}$ ($V = V^B$ in Fig. 8(a)), (c) $t_1 = 24 \text{ mm}$ ($V = V^B$ in Fig. 8(b)).

Figure 10 shows the diagram of 4 parameter model for DCI joints. Then, **Table 7** shows $\sqrt{area_{max}}$ estimated in previous section. In Fig. 10, the boundary of regions II and III is $\sqrt{area_{max}} \doteq 3000 \mu\text{m}$. In Table 7, since $\sqrt{area_{max}} < 3000 \mu\text{m}$ for the main plate thickness $t_1 = 6, 24 \text{ mm}$, Eq. (8) in the region II can be applied. Since $\sqrt{area_{max}} > 3000 \mu\text{m}$ for $t_1 = 12 \text{ mm}$, Eq. (10) in the region III can be applied. **Table 8** shows the parameters for drawing Fig. 10. Here, stress ratio R is calculated considering effect of compressive residual stress. As in our earlier study, compressive residual stress acting as the mean stress is -150 MPa . The compressive residual stress generated by shot blasting is the largest at the surface and decreases with the depth. Therefore, it is assumed that the effective compressive residual stress is approximately half of the residual stress measured on the surface.⁴⁾ On the above, stress ratio R is calculated from the fatigue limit in Fig. 6 and effec-

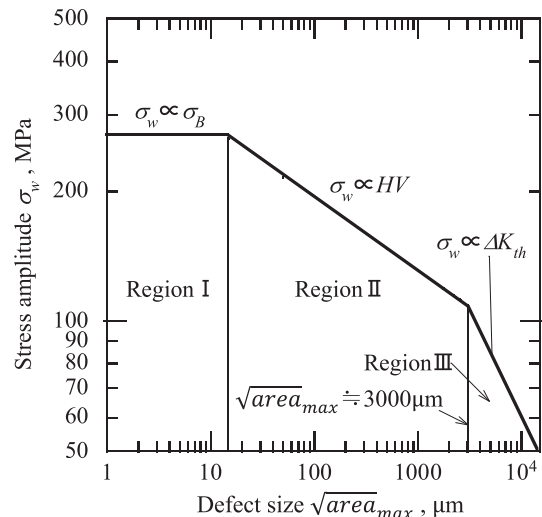


Fig. 10. 4 parameter model of DCI joints.

Table 7. The predicted maximum defect size: $\sqrt{area_{max}}$.

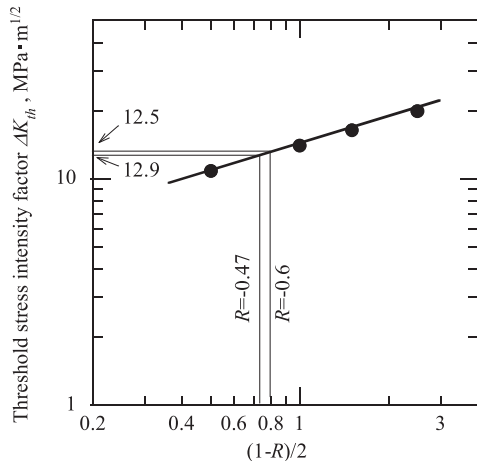
Main plate thickness t_1 (mm)	$\sqrt{area_{max}}$ (μm)
6	2 605
12	3 976
24	1 598

Table 8. Parameter value used for 4 parameter model.

Tensile strength σ_B (MPa)	Vickers hardness (HV)	Stress Ratio R	α	Threshold stress intensity factor ΔK_{th} (MPa \sqrt{m})
560	200*	$-0.47(t_1=6,24)$	0.38**	$12.5(t_1=6,24)$
		$-0.60(t_1=12)$		$12.9(t_1=12)$

*Converted value of Brinell hardness in Table 2

**Value at the long crack


Fig. 11. Relationship between ΔK_{th} and R for tension-compression fatigue tests.

tive compressive residual stress. As a result, when $t_1=6$, 24 mm, $R=-0.47$, when $t_1=12$ mm, $R=-0.60$ is obtained. In the range of these stress ratios, since 4 parameter model is almost the same, Fig. 10 shows in case of $R=-0.47$ on behalf of these. In addition, α is generally obtained by Eq. (9), but it is larger than the value sought by Eq. (9) depending on the material.²⁵⁾ Although, the value of ΔK_{th} is generally obtained by ΔK -decreasing tests, several studies have reported that this value is different from that obtained by ΔK -increasing tests.^{26,27)} Therefore, in this paper, the values of α and ΔK_{th} obtained by ΔK -increasing test of DCI were used.^{26,27)} 0.2% proof stress, tensile strength and elongation of DCI are almost the same as those of DCI joints. Because there is no data of ΔK_{th} at $R=-0.47$ and -0.60 , it is obtained by the relationship between ΔK_{th} and R in the case of the long crack whose size $\sqrt{area}=1\,850\,\mu\text{m}$ in Fig. 11. Here, $\sqrt{area}>1\,000\,\mu\text{m}$, ΔK_{th} is constant.^{26,27)} Therefore, the value of ΔK_{th} in Fig. 11 can be applied in region III, $\sqrt{area}_{max}>3\,000\,\mu\text{m}$.

Table 9 shows the lowest fatigue limit of DCI joint $\Delta\sigma_{low}^{DCI}$ obtained by Eqs. (8), (10) and Table 8. In this table, reduction rate C_r for the fatigue limit in Fig. 6 is shown together. When the main plate thickness $t_1=6$ mm, $\Delta\sigma_{low}^{DCI}=216$ MPa. When $t_1=12$ mm, $\Delta\sigma_{low}^{DCI}=178$ MPa. When $t_1=24$ mm, $\Delta\sigma_{low}^{DCI}=156$ MPa. Here, the fatigue limit of $t_1=24$ mm is 0.67 times that of the smooth specimens.⁴⁾ This is because the fracture position of the specimens for $t_1=24$ mm is the fillet portion where the stress is concentration (at A in Fig. 7). Therefore, the fatigue limit of the smooth specimens $\Delta\sigma_{low}^{DCI}=234$ MPa is obtained by Eq. (8). Then, $\Delta\sigma_{low}^{DCI}=156$ MPa at A (See Fig. 7) is calculated by multiplied $\Delta\sigma_{low}^{DCI}=234$ MPa by 0.67. On the above, the

Table 9. Lowest fatigue limit of DCI joints.

Main plate thickness t_1 (mm)	Lowest fatigue limit $\Delta\sigma_{low}^{DCI}$ (MPa)	Fatigue limit in Fig. 6 $\Delta\sigma_{exp}^{DCI}$ (MPa)	Reduction ratio $\Delta\sigma_{low}^{DCI} / \Delta\sigma_{exp}^{DCI}$ (%)
6	216*	220	98
12	178**	240	74
24	156***	220	70

*Calculated from Eq. (8)

**Calculated from Eq. (10)

***Calculated from Eq. (8) multiplied by 0.67

estimated lowest fatigue limit is decreased to 70% of the experimentally fatigue limit $\Delta\sigma_{exp}^{DCI}$.

6. Comparison of Lowest Fatigue Limit Considering the Largest Defects for DCI Joints with the Fatigue Limit of Welded Joints

6.1. Comparison of Lowest Fatigue Limit Obtained by Statistics of Extremes for DCI Joints with the Fatigue Limit of Welded Joints

Figure 12 shows the result of comparing the fatigue strength of DCI joints with the cross welded joints. The fatigue limit of DCI joints $\Delta\sigma_{low}^{DCI}$ is maximum and minimum values of the lowest fatigue limit in Table 9. The slope of the S - N diagram of DCI joint is assumed to be the same as that of the S - N diagram of $t_1=24$ mm (See Fig. 6(c)). The lowest fatigue limit of the cross welded joints $\Delta\sigma_{low}^{JSSC}$ is that of the fatigue design curve JSSC-E (See Fig. 3). In Fig. 12, $\Delta\sigma_{low}^{DCI}=156$ to 216 MPa. It is 2.5 to 3.5 times of $\Delta\sigma_{low}^{JSSC}=62$ MPa. On the above, although the fatigue strength of DCI joints is decreased by the defect, it is larger than that of the cross welded joints.

6.2. Lowest Fatigue Limit by Assuming that the Maximum Defect Predicted at other Portion Exists at the Maximum Stress Concentration Portion

In Table 9, when $t_1=24$ mm, the lowest fatigue limit of DCI joint is obtained as $\Delta\sigma_{low}^{DCI}=156$ MPa. Here, this value $\Delta\sigma_{low}^{DCI}=156$ MPa is estimated from the defect distribution appeared at the fillet portion A in Fig. 7 without considering the defects at the gripping portion C in Fig. 7. This is because dimensions of the same type of defects appearing at the same portion are usually used in statistics of extremes without using the defects appearing at different portions.¹⁵⁾

In this section, the maximum defect size is estimated from the total data of inclusion size at portion A, B, C. This is because the defects at portion C is excessively larger than the defects at portion A as shown in Table 5. Then, the obtained maximum defect size \sqrt{area}_{exc} is assumed to appear at the fillet portion A where the maximum stress concentration occurs. This maximum defect size \sqrt{area}_{exc} is estimated in a special way different from normal statistics of extremes. Then, the excessively lowest fatigue limit $\Delta\sigma_{exc}^{DCI}$ at portion A assuming that the maximum defect will be obtained to be compared with the fatigue limit of the cross welded joints.

From the total data of inclusion size at portion A, B, C, the maximum defect size $\sqrt{area}_{exc}=2\,840\,\mu\text{m}$ is obtained.

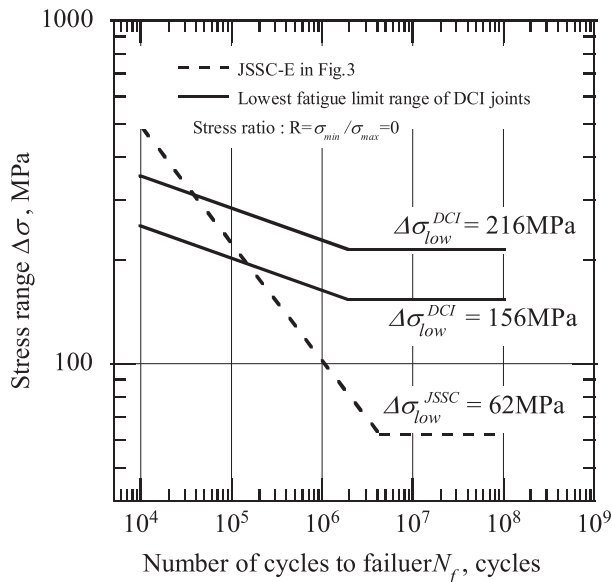


Fig. 12. Comparison of lowest fatigue limit of DCI joints and JSSC-E in Fig. 3.

This is about twice as larger as $\sqrt{area}_{max} = 1598 \mu\text{m}$ obtained from the data of inclusion size at portion A (See Table 7). Then, the lowest fatigue limit $\Delta\sigma_{exc}^{DCI} = 142 \text{ MPa}$ is obtained, which is about 10% lower than $\Delta\sigma_{low}^{DCI} = 156 \text{ MPa}$ in Table 9. However, $\Delta\sigma_{exc}^{DCI} = 142 \text{ MPa}$ is still more than 2 times larger than the lowest fatigue limit of the cross welded joint $\Delta\sigma_{low}^{JSSC} = 62 \text{ MPa}$.

7. Conclusion

Our previous study⁴⁾ showed that the fatigue strength of DCI joint was larger than that of the welded joint when the main plate thickness $t_1 = 24 \text{ mm}$. However, the defect size was not considered although many defects are included in DCI joints. In this study, therefore, the lowest fatigue strength of DCI joints $\Delta\sigma_{low}^{DCI}$ was estimated by using statistics of extremes. Then, $\Delta\sigma_{low}^{DCI}$ was compared with the lowest fatigue strength of the cross welded joint $\Delta\sigma_{low}^{JSSC}$ in Fig. 3. The conclusions can be summarized as follows:

(1) The lowest fatigue strength of DCI joints $\Delta\sigma_{low}^{DCI} = 156 \text{ MPa}$ estimated in this study is about 70% of the fatigue strength $\Delta\sigma_{exp}^{DCI} = 220 \text{ MPa}$ experimentally obtained. However, $\Delta\sigma_{low}^{DCI} = 156 \text{ MPa}$ is still 2.5 times larger than the lowest fatigue strength of cross welded joint $\Delta\sigma_{low}^{JSSC} = 62 \text{ MPa}$ prescribed by Japanese Society of Steel Construction (JSSC).

(2) The fatigue strength of cross welded joint decreases by about 40 MPa with increasing main plate thickness from $t_1 = 9 \text{ mm}$ to $t_1 = 20 \text{ mm}$. On the other hand, the fatigue strength of DCI joint is almost constant independent from the main plate thickness range $t_1 = 6 \text{ mm} \sim 20 \text{ mm}$. The reason can be explained from the stress concentration.

(3) DCI joint is fractured from the defects at the smooth section of the specimen when main plate thickness $t_1 = 6$,

12 mm. When $t_1 = 24 \text{ mm}$, it is fractured from the defects at the fillet portion of rib cross-section. The fractured position is controlled by the magnitude of stress intensity factor $K_I = K_1 \sigma_{w0} \sqrt{\pi \sqrt{area}}$, which represents the severity for the defect (See Table 6).

Acknowledgments

We thank Prof. Y. Murakami of the Kyushu University for his thoughtful and helpful comments about statistics of extremes.

This research was conducted by FY 2017 subsidies for basic research (Saga prefecture technology promotion support technology industry, academia and government collaboration technological innovation support project). We express our deep appreciation.

REFERENCES

- 1) I. Ovali, V. Kilicli and M. Erdogan: *ISIJ Int.*, **53** (2013), 375.
- 2) R. M. Ghergu, J. Sertucha, Y. Thebault and J. Lacaze: *ISIJ Int.*, **52** (2012), 2036.
- 3) S. Lu, X. Wang, W. Dong and Y. Li: *ISIJ Int.*, **53** (2013), 96.
- 4) T. Hidaka, N. A. Noda, Y. Sano, N. Kai and H. Fujimoto: *ISIJ Int.*, **59** (2019), 1860. <http://doi.org/10.2355/isijinternational>. ISIJINT-2019-237
- 5) M. Kamakura, M. Nihei, E. Sasaki, M. Kanao and M. Inagaki: *J. Jpn. Weld. Soc.*, **48** (1979), 1060 (in Japanese).
- 6) T. Okada, N. Yamamoto and M. Mouri: *Kanrin*, **60** (2015), 27 (in Japanese).
- 7) K. Anami and C. Miki: *J. Steel Constr. Eng.*, **4** (1997), 9.
- 8) Japanese Society of Steel Construction: Fatigue Design Recommendations for Steel Structures, Gihodo Shuppan Co., Ltd., Tokyo, (2012), 28 (in Japanese).
- 9) G. B. Marquis and Z. Barsoum: *Procedia Eng.*, **66** (2013), 98.
- 10) T. Mori, K. Minami and Y. Kabuto: *J. Steel Constr. Eng.*, **18** (2011), 71.
- 11) The Society of Materials Science, Japan: Handbook of Fatigue Design, Yokendo Ltd., Tokyo, (2005), 6 (in Japanese).
- 12) Y. Murakami: Metal Fatigue Effects of Small Defects and Nonmetallic Inclusions, Yokendo Ltd., Tokyo, (2014), 17 (in Japanese).
- 13) Y. Murakami and C. Sakae: *J. Soc. Mater. Sci. Jpn.*, **41** (1992), 1214 (in Japanese).
- 14) Y. Murakami and M. Ishida: *Trans. Jpn. Soc. Mech. Eng.*, **50** (1984), 1359 (in Japanese).
- 15) Y. Murakami, H. Machida, S. Miyakawa and T. Takagi: *Trans. Jpn. Soc. Mech. Eng.*, **83** (2017), 1 (in Japanese).
- 16) Y. Murakami: Metal Fatigue Effects of Small Defects and Nonmetallic Inclusions, Yokendo Ltd., Tokyo, (2014), 242 (in Japanese).
- 17) Y. Murakami: Metal Fatigue Effects of Small Defects and Nonmetallic Inclusions, Yokendo Ltd., Tokyo, (2014), 235 (in Japanese).
- 18) H. Masuo, Y. Tanaka, S. Morokoshi, H. Yagura, T. Uchida, Y. Yamamoto and Y. Murakami: *Int. J. Fatigue*, **117** (2018), 163.
- 19) Y. Murakami and K. Matsuda: *Trans. Jpn. Soc. Mech. Eng. A*, **52** (1986), 1492 (in Japanese).
- 20) Y. Murakami and M. Endo: *Trans. Jpn. Soc. Mech. Eng. A*, **49** (1983), 127 (in Japanese).
- 21) Y. Murakami and M. Endo: *J. Soc. Mater. Sci. Jpn.*, **35** (1986), 911 (in Japanese).
- 22) Y. Sugiyama, K. Asami and S. Matsuoka: *Trans. Jpn. Soc. Mech. Eng. A*, **58** (1992), 2287 (in Japanese).
- 23) H. Tamura, Y. Sugiyama, N. Shiraki, K. Matsuzaka, T. Umehara and H. Usami: *J. JFS*, **73** (2001), 605 (in Japanese).
- 24) Y. Murakami: Metal Fatigue Effects of Small Defects and Nonmetallic Inclusions, Yokendo Ltd., Tokyo, (2014), 63 (in Japanese).
- 25) Y. Kondo, C. Sakae, M. Kubota and T. Kudou: *Fatigue Fract. Eng. Mater. Struct.*, **26** (2003), 675.
- 26) J. Yamabe and M. Kobayashi: *Trans. Jpn. Soc. Mech. Eng. A*, **71** (2005), 1508 (in Japanese).
- 27) J. Yamabe and M. Kobayashi: *J. Solid Mech. Mater. Eng.*, **1** (2007), 667.